New ultra-violet and near-infrared blocking filters for energy saving applications: fabrication of tantalum metal atom cluster-based nanocomposite thin films by electrophoretic deposition

Thi Kim Ngan Nguyen, Adele Renaud, Maxence Wilmet, Noee Dumait, Serge Paofai, Benjamin Dierre, Wanghui Chen, Naoki Ohashi, Stephane Cordier, Fabien Grasset, et al.

▶ **To cite this version:**

Thi Kim Ngan Nguyen, Adele Renaud, Maxence Wilmet, Noee Dumait, Serge Paofai, et al.. New ultra-violet and near-infrared blocking filters for energy saving applications: fabrication of tantalum metal atom cluster-based nanocomposite thin films by electrophoretic deposition. Journal of Materials Chemistry C, 2017, 5 (40), pp.10477-10484. 10.1039/c7tc02454a . hal-01631913

HAL Id: hal-01631913
https://univ-rennes.hal.science/hal-01631913

Submitted on 24 Nov 2017

HAL is a multi-disciplinary open access archive for the deposit and dissemination of scientific research documents, whether they are published or not. The documents may come from teaching and research institutions in France or abroad, or from public or private research centers.

L'archive ouverte pluridisciplinaire **HAL**, est destinée au dépôt et à la diffusion de documents scientifiques de niveau recherche, publiés ou non, émanant des établissements d'enseignement et de recherche français ou étrangers, des laboratoires publics ou privés.

New ultra-violet and near-infrared blocking filters for energy saving applications: fabrication of tantalum metal atom cluster-based nanocomposite thin films by electrophoretic deposition†

Thi Kim Ngan Nguyen,‡[abc] Adèle Renaud,‡*[d] Maxence Wilmet,[ad] Noée Dumait,[d] Serge Paofai,[d] Benjamin Dierre,[ae] Wanghui Chen,[abc] Naoki Ohashi,[ace] Stéphane Cordier,[d] Fabien Grasset*[ace] and Tetsuo Uchikoshi*[abc]

This study reports the first integration of inorganic tantalum octahedral metal atom clusters into multifunctional nanocomposite coating materials and devices for window technology and energy saving applications. $[Ta_6Br^i_{12}]^{n+}$ (n = 2, 3 or 4) cluster-based high visible transparency UV and NIR filters are realized. Green and brown colored films are fabricated by coating on an indium-doped tin oxide glass substrate by electrophoretic deposition, an industrialized solution process. The efficiency in energy saving of the new UV-NIR filters was estimated by the determination of different figure of merit (FOM) values, such as T_{vis}, T_{sol} and T_{vis}/T_{sol} (T_{sol} = solar transmittance and T_{vis} = visible transmittance), and the color coordinates (x, y, z and L^*a^*b). The T_{vis}/T_{sol} ratio is equal to 1.25 for the best films. Such values are evidence of a higher energy saving efficiency than most of the inorganic composites reported in the literature. These promising results pave the way for the use of transition metal clusters as a new class of nanocoatings in energy saving window-based applications.

A Introduction

In the general context of energy saving due to the increase in energy consumption and serious environmental problems induced by global warming,[1] the realization of low-cost selective films as an ultra-violet (UV) and near-infrared (NIR) barrier with a high visible transparency is a field of research of growing interest.[2] Integrated into window technology, these transparent coating materials should be able to reduce (i) the exposure to UV, which can mainly result in the strong degradation of organic matter (*i.e.*, polymer or plants) and/or (ii) the energy consumption for buildings (houses, greenhouses, *etc.*) or vehicles, thanks to better thermal insulation by controlling the NIR solar radiation. Indeed, the solar energy distribution on the earth's surface (after absorption through the atmosphere) is composed of approximately 5% UV radiation (300–400 nm), 43% visible radiation (400–700 nm) and approximately 52% NIR radiation (700–3000 nm). Thus almost half of the solar energy comes from infrared radiation, and particularly from the highest thermal energy region, namely from 700 to 1100 nm.[2] Considering window technology, an efficient heat barrier window should exhibit a high transparency in the visible wavelength domain and block NIR radiation as much as possible to reduce heat transfer. So far, solar-glass control devices can be defined as dynamic or static materials. The commonly used dynamic products (also called smart windows) are electrochromic devices using the same organization as a thin-film electrical battery. Another efficient approach for the fabrication of dynamic windows seems to use the plasmonic effect of doped metal oxide nanocrystals.[2] Regarding static devices, which are the targets of this study, commercial products are generally based on reflective multi-layer structures including at least a noble metal (mainly Ag) mainly deposited by a vacuum process.[2] They block thermal radiation by reflection with low energy transfer in the material. Conversely, absorbing materials appear as complementary energy-saving materials of interest due to their ability to be used in several ways *i.e.*, (i) to block the UV radiation and (ii) to block a portion of the NIR radiation by absorbing and re-emitting this outdoor heat (efficient for warm climate zones) and/or (iii) to convert a portion of the sunlight to thermal energy or electric power (efficient for colder climate zones).[2,3] Nowadays, popular NIR absorptive materials are composed of a

[a] *CNRS-Saint Gobain-NIMS, UMI 3629, Laboratory for Innovative Key Materials and Structures (LINK), National Institute of Material Science, 1-1 Namiki, Tsukuba 305-0044, Japan. E-mail: GRASSET.Fabien@nims.go.jp, fabien.grasset@univ-rennes1.fr*

[b] *Fine Particles Engineering Group, RCFM, National Institute of Material Science, 1-2-1 Sengen, Tsukuba 305-0047, Japan. E-mail: UCHIKOSHI.Tetsuo@nims.go.jp*

[c] *RCFM, National Institute for Materials Science, 1-1 Namiki, Tsukuba, Ibaraki 305-0044, Japan*

[d] *Université de Rennes 1, UMR Institut des Sciences Chimiques de Rennes UR1-CNRS 6226, Equipe Chimie du Solide et Matériaux, 263 av. du Général Leclerc, 35042 Rennes, France. E-mail: adele.renaud@univ-rennes1.fr*

[e] *NIMS-Saint-Gobain Center of Excellence for Advanced Materials, National Institute of Material Science, 1-1 Namiki, Tsukuba, Ibaraki 305-0044, Japan*

† Electronic supplementary information (ESI) available. See DOI: 10.1039/c7tc02454a

‡ Ms N. T. K. Nguyen and Dr A. Renaud made equal contributions in this study.

revised manuscript

few metal oxides,[4] a composite materials[5] or organic materials such π-conjugation systems or metal complexes.[6] However, most of them are not really efficient for UV blocking, and inorganic materials are mainly deposited on a transparent substrate by a physical method as reported by several groups.[4,5] Currently, replacement of the noble metal and use of solution processes are highly desirable in order to reduce the cost of these materials.[4,5] In this context, we recently demonstrated the first integration of tantalum octahedral cluster compounds, $K_4Ta_6Br_{18}$ (denoted as KTB), in multifunctional nanocomposite materials for window technology devices.[6] This preliminary work explored the ability to dynamically control the optical properties by the fabrication of the first Ta_6-based electrochromic cell. This cell consisted of two electrodes separated by a liquid electrolyte containing the Ta_6 cluster. Nevertheless, the occurrence of bubbles during color modification clearly indicated a redox process involving the solvent. This appears to be necessary to explore new deposition solution processes able to fabricate a solid thin-layer coating with controlled thickness and investigate the influence of the solvent. In this paper, for the first time we propose the fabrication of a Ta_6-based solid thin film by using an electrophoretic deposition (EPD) process. This method is widely used on a large variety of materials such as oxides,[7] carbonated materials,[8] organic or hybrid compounds[9] or metals.[10] Its low cost, and the fact that it is easy to set up and easy to control the film thickness make this deposition technique very convenient for producing film coatings with a short deposition time.[11] To achieve this new goal, a hexanuclear metal atom cluster compound $[(Ta_6Br_{12})Br_2(H_2O)_4]\cdot 3H_2O$ (denoted as TBH) was used instead of KTB as previously reported.[6]

The metal atom cluster family has been known for a long time and is composed of clusters of a few atoms with a nanometer size (under 2 nm), which induces specific electronic structures and thus unique properties.[12–15] These hexanuclear metal atom clusters consist of a cluster of six metal atoms attached by metal–metal bonds, thus forming an octahedron. This metallic octahedron is bound by eight face-capping and six terminal apical ligands or twelve edge-bridged inner ligands and six terminal apical ligands (see Fig. 1 with the $[Ta_6L^i_{12}L^a_6]^{2+}$ cluster as an example). The face-capped cluster units, such as $[Mo_6L^i_8L^a_6]^{n-}$ (L^i, L = Cl, Br, I; L^a, L = F, Cl, Br, I, H_2O, OH, CN...), are mostly studied for their optoelectronic properties (large Stokes shift, deep red-NIR luminescence, strong absorption in the visible spectrum) affording a wide set of potential applications in biotechnological devices,[16] optical devices,[17] catalysis,[18] photovoltaic cells,[19] *etc.* The $[(M_6L^i_{12})L^a_6]^{n-}$ cluster units are notable because of the $(M_6L^i_{12})^{n+}$ cluster core, which exhibits physicochemical behaviors of great interest such as catalytic properties,[20] a wide structural variety[21] and a strong redox activity in combination with strong UV-vis-NIR absorption properties.[22] More particularly, the tantalum cluster cores, $[Ta_6Br^i_{12}]^{2+}$, are known as a commercial tool for phase determination of large biological assemblies by X-ray crystallography,[23] as radiographic contrast agents[24] and as a deep green-emerald color pigment.[25] Moreover, it is known that these units can be reversibly oxidized to $[Ta_6Br^i_{12}]^{3+}$ and $[Ta_6Br^i_{12}]^{4+}$ causing drastic modulation of the optical properties in the UV-vis-NIR range to afford red-brownish solutions.[26–28] Based on this knowledge, we applied the concept of nanoarchitectonics,[29] namely multifunctional systems achieved by the combination of several materials in a well-defined architecture, for the design of new materials targeting energy saving applications. Furthermore, we report the first manufacture of UV-NIR protective transparent films based on the functionalization of an IR reflector window (glass coated by a transparent conductive oxide (TCO) (indium doped tin oxide (ITO))) with a $[Ta_6Br^i_{12}]^{2+}$cluster-based NIR absorber, allowing the absorption of the most energetic IR radiation (700–1100 nm) and the selectivity of the least energetic IR radiation (1100–3000 nm) by the TCO. Thus, the objective of this study is to introduce the feasibility of preparing colored and transparent solid nanocomposite films composed of Ta_6 clusters by using the EPD process for static window technology. The next step will be to upgrade these results to dynamic devices.

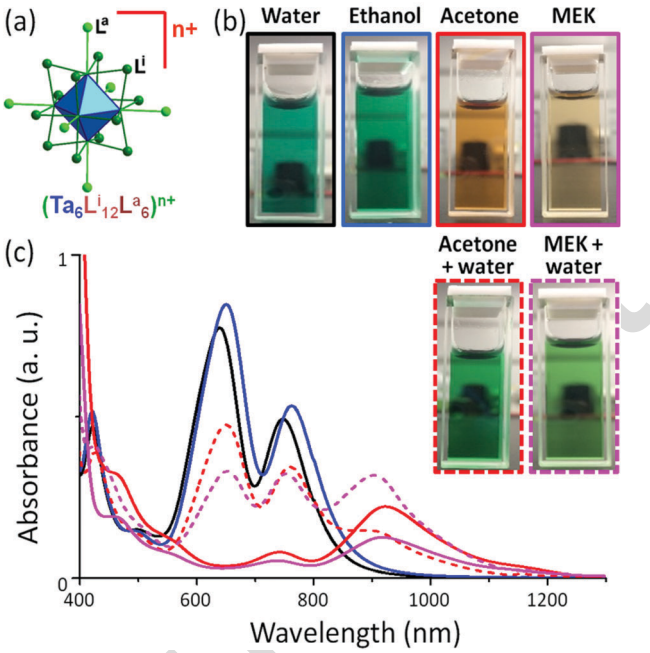

Fig. 1 (a) Representation of the tantalum octahedral cluster cation $[Ta_6X^i_{12}L^a_6]^{n+}$. L^i and L^a correspond to the inner and apical ligands, respectively; (b) photographs of EPD solutions containing TBH powder dissolved in water, ethanol, acetone, MEK, water/acetone and water/MEK; (c) UV-vis-NIR absorption spectra of these EPD solutions.

B Materials and methods

The KTB compound was obtained by solid state synthesis using a well-known protocol developed by Koknat *et al.*[30] The detailed synthesis and characterization of KTB were reported in ref. 6. The green TBH powder, containing $[Ta_6Br^i_{12}]^{2+}$ cluster cores, was obtained from the KTB powder compound dissolved in water at 80 °C under an argon atmosphere in addition to HBr and $SnBr_2$ according to a previously reported method.[30] After several hours of stirring, the green solution is filtered to remove the non-dissolved particles (mostly tantalum powder), then the TBH green powder was recrystallized. An outline of the

Revised manuscript

preparation of KTB and TBH is presented in the ESI† (Scheme S1). Reagent grade chemicals, distilled water (Water Purifiers WG710, conductance of 0.5×10^{-4} S m^{-1} at 25 °C), acetone (99.5%), methyl ethyl ketone (MEK, 99%), ethanol (99.5%) and poly(vinylpyrrolidone) (PVP, M_w = 40 000 g mol^{-1}) were used without any purification treatment. ITO glass (Geomatec Co., Ltd (Japan), 6–8 Ohm sq^{-1}), washed with distilled water and acetone during ultrasonication, was connected to a Keithley Model 2400 Series SourceMeter as the anodic or cathodic substrate and a stainless steel sheet as the counter electrode. Voltages from 8 to 30 V and deposition times from 20 to 90 s were applied. All the experimental parameters are reported in Tables S1 and S2 in the ESI.† The microstructure of the powder and thin films was studied by several complementary techniques, *i.e.*, X-ray diffraction (XRD) measurements were performed using a Rigaku Ultima 3, Rint 2000 diffractometer at 40 kV and 30 mA in the 2θ angle range from 5° to 50° with Cu Kα radiation (λ = 1.54 Å). The Raman scattering spectra of the TBH powder and Ta_6@PVP@ITO films were measured using a LabRam High Resolution spectrometer coupled to a confocal microscope (Horiba Jobin Yvon), 600 g mm^{-1} grating and 10× objective. A He–Ne 633 nm laser was used as an excitation source. The Raman spectra were recorded at room temperature with 100 s exposure time and 2 accumulations. Field emission-scanning electron microscopy (FE-SEM) images were obtained using a JEOL JSM 6301F microscope operating at 7 kV. The XRD, Raman and SEM characterizations of the TBH powder is reported in the ESI† (Fig. S1–S3). Scanning transmission electron microscopy (STEM) images of the film were taken using a Cs-corrected JEOL JEM2100F microscope operating at 200 kV. This is equipped with a field-emission electron gun and incorporated with multiple additional functions (an energy-dispersive spectrometer (EDX) and a high sensitivity *Z*-contrast high angle annular dark field (HAADF) detector). Optical absorbance of the solution and transmittance of the films were measured by UV-vis-NIR spectroscopy (Jasco V570) in the wavelength range of 220 nm to 2000 nm at a scan rate of 400 nm s^{-1}.

C Results and discussion

C-1 TBH in solution

TBH was preferred to KTB because its solubility limit is higher in many solvents. The XRD pattern is reported in Fig. S1 in the ESI.† The powder contains micron-sized rod-like crystallites as observed by SEM (Fig. S2 in the ESI†). This starting material is used as a precursor of the $[Ta_6Br^i_{12}]^{2+}$ cluster core for the design of $[Ta_6Br^i_{12}(H_2O)^a_6]^{2+}$ cluster unit based compounds as demonstrated by Sokolov *et al.*[30] The presence of the $[Ta_6Br^i_{12}]^{2+}$ cluster core was clearly confirmed by XRD and Raman spectroscopy (Fig. S1 and S3 in the ESI†). Thus, various common solvents (distilled water, ethanol, acetone and MEK) were selected as the dispersing media of the TBH compound to obtain green stable and transparent solutions for the EPD process (Table S1 in the ESI†). On the one hand, the color of the solution was deep emerald-green in water and olive-green in ethanol after stirring for a few minutes (Fig. 1b). On the other hand, the solution was red-brown in acetone and MEK and required a long stirring time before complete dissolution of the TBH powder (Fig. 1b). Actually, after dispersion of the precursor, the ketone-based solutions are turbid and exhibited a greenish color that turned to turbid olive-green and finally to a clear red-brown color after 48 h. This behavior clearly indicated the oxidation of the initial $[Ta_6Br^i_{12}]^{2+}$ containing cluster cores of the $[Ta_6Br^i_{12}]^{3+}$ or $[Ta_6Br^i_{12}]^{4+}$ species during the dissolution process of TBH (see Table S3 in the ESI†).[24–27] Indeed, as already published, the green-emerald color is attributed to the presence of $[Ta_6Br^i_{12}]^{2+}$. Moreover, electrochemical studies showed that these species can be involved in two reversible one-electron oxidation processes to successively form the $[Ta_6Br^i_{12}]^{3+}$ and $[Ta_6Br^i_{12}]^{4+}$ species.[31,32] The UV-vis-NIR absorption of the 6 solutions are reported in Fig. 1b. Optically, the changing of color is due to the appearance of new absorption bands in the UV-NIR region and a decrease of their intensity in the visible region to afford brownish solutions (Fig. 1c).[27,33] According to Cooke *et al.*,[31] the constant of the reproportionation reaction corresponding to $[Ta_6Br^i_{12}]^{2+} + [Ta_6Br^i_{12}]^{4+} \rightarrow 2[Ta_6Br^i_{12}]^{3+}$ has a relatively high calculated value which could suggest that the $[Ta_6Br^i_{12}]^{3+}$ oxidized species are more stable in solution than the $[Ta_6Br^i_{12}]^{4+}$ ones.

We assume that the red-brown color of the solutions corresponds to the $[Ta_6Br^i_{12}]^{3+}$ species and the green ones certainly correspond to the $[Ta_6Br^i_{12}]^{2+}$ species. In contrast, for the $[Mo_6Br_{14}]^{2-}$ species,[34] which is stable in MEK and acetone solvents, it seems clear that during dissolution, the $[Ta_6Br^i_{12}]^{2+}$ species undergo oxidation in these solvents and that should be detrimental to achieving green films. However, we already determined that acetone or MEK are the best solvents for the EPD process of the $[Mo_6Br_{14}]^{2-}$ based cluster compounds.[34] Thus, in order to stabilize or at least reduce the kinetics of oxidation in the ketone solvents, we first dissolved TBH in a small amount of water before the addition of acetone and MEK.

As reported in Fig. 1 and Table S1 in the ESI,† the best green solution was obtained by the mixture of water and acetone. Ten mg of the TBH green powder was dissolved in water (from 0.15 to 0.5 mL of water) and diluted by the addition of 10 or 15 mL of acetone (see Table S2 in the ESI†). A 40′ sonication is necessary to obtain a clear green dispersion leading to a much better stabilization of the $[Ta_6Br^i_{12}]^{2+}$ species (Fig. 1b). In this specific case, it is possible to maintain the green color for several days at room temperature before the progressive oxidation occurs. In other words, to reduce the kinetics of oxidation, it is important to add a small amount of water before acetone, otherwise the dissolution takes a long time and leads to a red-brown solution. A further study is necessary to totally determine the mechanism of this redox process.

C-2 Thin film preparation and morphology characterization

EPD experiments (Fig. 2a) were conducted using each of these solutions after a filtration process (0.2 μm). The deposition results are listed in Tables S1 and S2 in the ESI.† The films were formed at different applied voltages and deposition times in order to optimize the conditions. The differences between the

Revised manuscript

solvents are certainly induced by different factors such as the surface states of the electrodes in the solutions, the solvation shell of the cluster, the variation in the dissociation degree of the precursor according to the solvent which affects the conductivity of the solutions or the difference in the mobility of the clusters units (or counter ions).[34]

The best depositions were performed in acetone without (named brown-Ta_6@ITO) and with water (named green-Ta_6@ITO) (see the deposition conditions in Table S2 in the ESI†). As expected from the solution, red-brown transparent films (Fig. 2b) were obtained in acetone without water, while forming a green one in acetone with water (Fig. 2c). Green-Ta_6@ITO was deposited on the cathode (negatively charged) in good agreement with the positive charge of the Ta_6 cluster, whereas surprisingly brown-Ta_6@ITO was formed on the ITO anode side (positively charged). This result clearly indicated the presence of an anionic form in the red-brown solution which could be explained by the total or partial exchange of the apical ligands (Br and/or H_2O) by the OH^- or $(CH_3)_2CO^-$ groups as already observed for the Mo_6 clusters.[34]

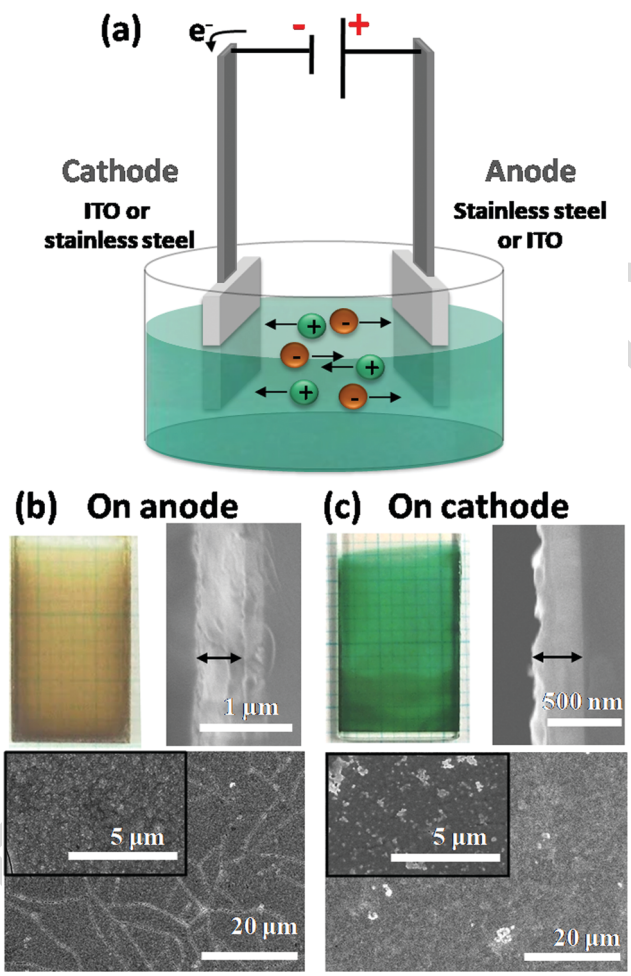

Fig. 2 (a) Schematic representation of anodic (ITO on the anode and stainless steel on the cathode) or cathodic (ITO on the cathode and stainless steel on the anode) EPD; (b) photograph and SEM images of the cross section and surface of the brown-Ta_6@ITO film (25 V and 60 s); (c) photograph and SEM images of the cross section and surface of the green-Ta_6@ITO film (20 V and 60 s).

The green color of the films, obtained from the water/acetone solution, clearly suggests that the $[Ta_6Br^i_{12}]^{2+}$ cluster core does not participate in the redox process. Thus we can postulate that the cluster charge is especially balanced with the ITO cathode charge.[35] However, other processes can occur on the cathode such as the reduction of water to produce hydroxide anions and hydrogen (E° = −0.83 V/NHE). These ions may interact with the Ta_6 clusters, and in addition the strong electrostatic interaction between the electrode and clusters may ensure the immobilization of the clusters on the electrode surface, at least for the first layers.[24,36] For the following layers, the hydrogen layers between the H_2O ligands of the clusters,[12] van der Waals interactions between the halogens or/and the condensation of the clusters should help with the film cohesion.

The morphology of both films was characterized by SEM investigations. The films have average thicknesses of around 500 nm and 300 nm for the brown and green films, respectively, as observed in the SEM images of the cross section of Fig. 2b and c. These Fig. 2b and c show the surface of both films with some roughness and cracks, and in the case of the green-Ta_6@ITO film some agglomerates without well-defined shapes are dispersed on the surface.

C-3 Optical properties of thin films

Despite the lack of homogeneity, the transmittance of the brown-Ta_6@ITO films reached 66% at 780 nm in the visible range (Fig. 3). This corresponds to a transmission loss of around 15% compared with an ITO glass substrate due in particular to the absorption of the red-brown $[Ta_6Br^i_{12}]^{3+}$-based coating. It appears that the UV-vis-NIR behavior of the brown films is closer to the spectrum of $[Ta_6Br^i_{12}]^{4+}$ (in aqueous solution consisting of HBr) published by Spreckelmeyer *et al.*[28] than that of $[Ta_6Br^i_{12}]^{3+}$. The five peaks at 384, 453, 550, 729 and 892 nm of the brown films correspond to a blue shift compared to those of the initial red-brown solution (400, 468, 557, 745 and 933 nm). It seems possible under voltage to favor the $[Ta_6Br^i_{12}]^{4+}$ species instead of the $[Ta_6Br^i_{12}]^{3+}$ species. Nevertheless, even if the film is not green, this tantalum cluster-based coating is stable with time and leads to improving the NIR optical properties of the ITO substrate due to the additional NIR absorption peak at 892 nm.

The transmittance of the green-Ta_6@ITO film, as shown in Fig. 3, reached 60% at 550 nm in the visible range. Moreover, it comprises four main absorption peaks at 358, 429, 648 and 759 nm characterizing the $[Ta_6Br^i_{12}]^{2+}$ species and inducing the green film color. If acetone induces the oxidation of the initial cluster core in $[Ta_6Br^i_{12}]^{3+/4+}$, the presence of a small amount of water (up to a concentration of 0.015 mL of water per mL of acetone) during precursor dissolution leads to stabilization of $[Ta_6Br^i_{12}]^{2+}$ in solution and realization of the transparent green films.

We investigated the effect of water concentration on the optical properties of the films, and we found that a large amount of water drastically impacts the film transparency (see Fig. S1 in the ESI†).

manuscript

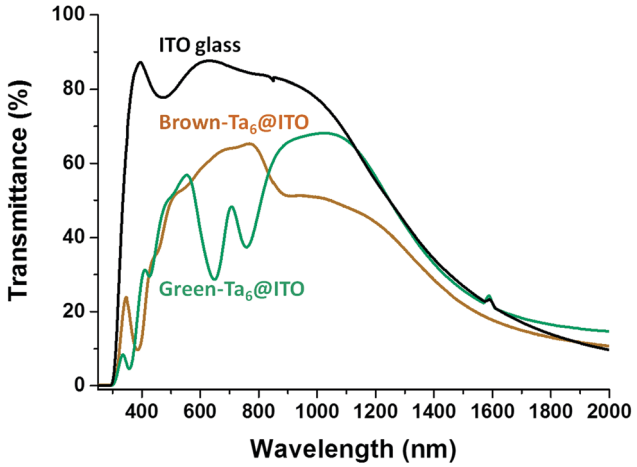

Fig. 3 UV-vis-NIR transmission spectra of the ITO substrate and the brown- and green-Ta_6@ITO films at 10 V and 60 s.

For this, the green-Ta_6@ITO films were prepared from solutions containing various water concentrations (from 0.02 to 0.050 mL of water per mL of acetone). For the same coating conditions (10 V during 60 s), an increase in the cloudiness of the films with an increase in water concentration was clearly observed. This decrease in transparency in the visible range was confirmed by UV-vis-NIR measurements (Fig. S1a in the ESI†). The morphology of the films was investigated by SEM in order to more deeply understand the origin of this scattering phenomenon. SEM photographs (Fig. S1b in the ESI†) highlight an increase in the particle size concomitant with the increase of the water content. The surface remains relatively smooth and homogeneous for the films prepared with 0.02 mL of water per mL of acetone. These surfaces are coated by some particle agglomerates not having the well-defined shapes. However, for higher concentrations (>0.025 mL mL^{-1} of acetone), the particle shape became bigger and better defined until a network of particles in the pellet form (1 μm × 200 nm) was created at a concentration of 0.05 mL of water per mL of acetone. This increase in particle size and surface roughness favors the scattering of light in all directions and limits the transmission of light through the Ta_6 films, which clearly explains the decrease in transparency. Although water is necessary in acetone to stabilize the green Ta_6 cluster species, it seems to favor particle growth and crystallization which limits the optical properties in the visible range. X-ray diffraction patterns depicted in Fig. S1c in the ESI† seem to confirm this increase in crystallinity of the tantalum cluster particles. In order to evaluate the efficiency of the cluster coating as an energy saving material, different figure of merit (FOM) values, T_{vis}, T_{sol}, and T_{vis}/T_{sol},[5] and the color coordinates (x, y, z and L^*a^*b) were calculated for each film (ITO, brown-Ta_6@ITO and green-Ta_6@ITO films). The solar transmittance, T_{sol}, is the integrated spectral transmittance of a window weighted with the normalized solar energy distribution spectrum. The visible transmittance, T_{vis}, was calculated in a similar way, but the solar transmittance is now weighted with the photopic response of the human eye (see the ESI† for more details).[5] The FOM values are reported in

Table 1 x, y, and z color coordinates and the FOM values of the ideal blocker, ITO glass substrate and the brown- and green-Ta_6@ITO films

Name	x	y	z	T_{vis}	T_{sol}	T_{vis}/T_{sol}
ITO 6–8 Ω sq^{-1}	0.318	0.340	0.342	87.6	76.2	1.15
Brown-Ta_6@ITO film 25 V 60 s	0.352	0.374	0.274	54.1	46.5	1.16
Green-Ta_6@ITO 20 V 60 s	0.326	0.361	0.313	50.6	41.8	1.21
Green-Ta_6@PVP@ITO 30 V 30 s	0.296	0.359	0.345	62.7	50.0	1.25
Green-Ta_6@PVP@ITO 30 V 60 s	0.284	0.382	0.334	50.4	41.0	1.23
Green-Ta_6@PVP@ITO 30 V 90 s	0.287	0.383	0.330	48.9	39.1	1.25
Ideal blocker	0.314	0.331	0.355	90.0	48.7	1.85

Table 1 and Fig. 4. The L^*a^*b color space values are reported in the ESI† (Tables S5 and S6).

When compared to ITO glass, both films clearly have an impact in terms of their color and UV-NIR solar energy attenuation. Indeed, the CIE value is shifted and the T_{vis}/T_{sol} ratio is higher for both films than that of ITO, especially for the green-Ta_6@ITO film with a value of 1.21. For the ideal visible transparent ((90%) between 400 and 780 nm) film absorbing 100% of UV (200–400 nm) and NIR (780–2000 nm) radiation, the value of the T_{vis}/T_{sol} ratio should be 1.85, but most of the composites reported in the literature have an experimental value close to 1.[5] The T_{vis} values are higher than 50%, which is the lower limit acceptable for window applications.[5]

Unfortunately, after a few days, while the color of the brown-Ta_6@ITO film is stable, the green-Ta_6@ITO films are slightly oxidized by air and lost their green color (Fig. S4 in the ESI†). Nevertheless, this change in the color did not affect the values of T_{vis}, T_{sol}, and T_{vis}/T_{sol} (see Table S4 in the ESI†).

C-4 UV-NIR blocking thin film optimization process

To overcome these negative effects during the deposition process, we investigated the incorporation of a polymer binder, *i.e.*, PVP, into the solution with a weight ratio of Ta_6/PVP = 1. The purpose of the addition of the polymer was (i) to increase the cluster dispersion and limit the Ta_6-based particle growth and light scattering, and (ii) to stabilize the green color with time by preventing the oxidation of the clusters. Indeed, it is known that PVP can serve as a surface stabilizer, a growth modifier, a nanoparticle dispersant, and a reducing agent.[37] An important feature of PVP is the existence of carbonyl oxygens which can hydrogen bond solvent molecules or clusters. Thus, we added 10 mg of PVP to the initial solution (consisting of 10 mg

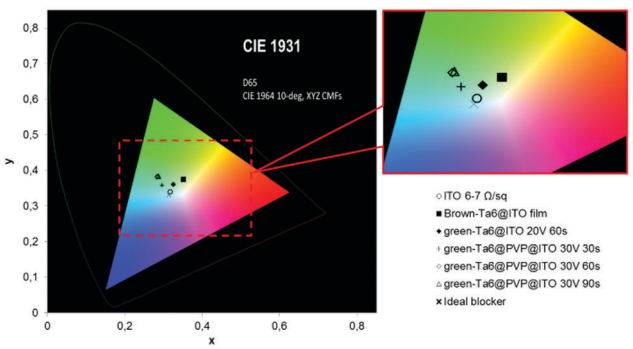

Fig. 4 CIE chromaticity coordinates of the ideal blocker, the ITO glass substrate and the brown- and green-Ta_6@ITO films.

Revised manuscript

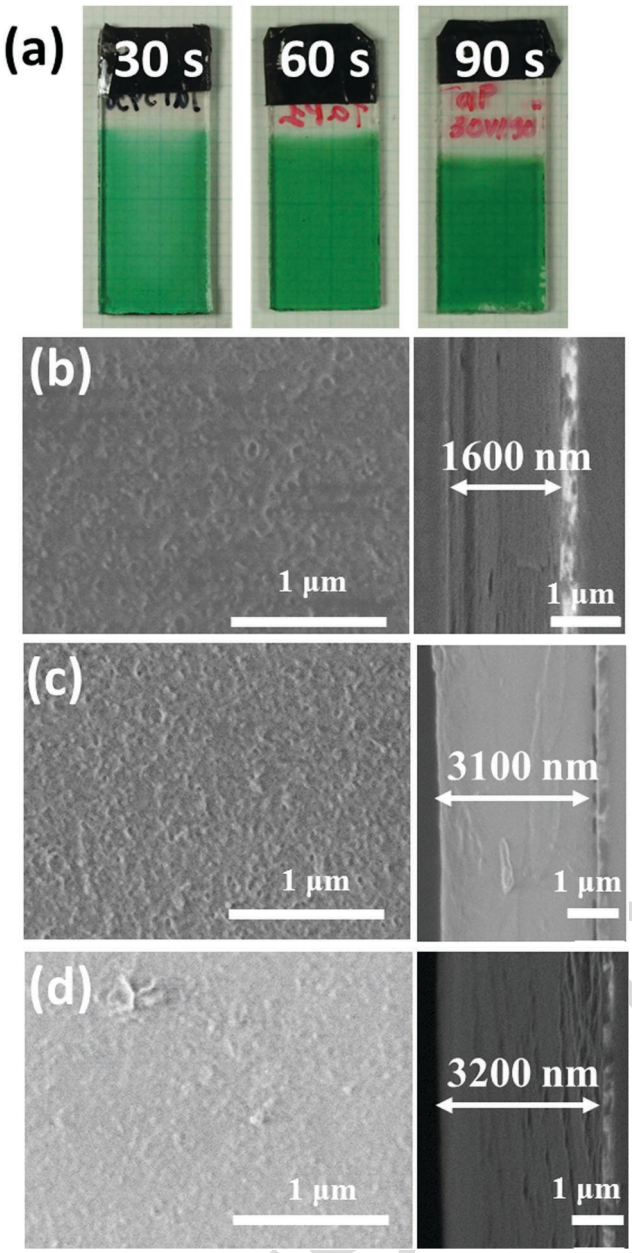

Fig. 5 (a) Photographs of 1 × 2.5 cm substrates and SEM images of green-Ta_6@PVP@ITO films on 1 × 2.5 cm substrates prepared at 30 V and 30 s (b), 60 s (c) and 90 s (d).

of the TBH green powder, 0.225 mL of water and 15 mL of acetone). Green transparent Ta_6@PVP@ITO films of around 1500 to 3000 nm (film photograph and cross section in Fig. 5) thickness were obtained by the EPD process on the cathode side at the optimized applied voltages and deposition times (30 V for 30 s, 60 s or 90 s). These films exhibited a high transmission in the visible range (Fig. 6) which is related to their smooth and homogeneous surfaces observed in the SEM images of Fig. 5. The homogeneous dispersion of the Ta_6 cluster without any large aggregates is demonstrated by STEM analysis (Fig. S5 and S6 in the ESI†). Similar to the bulk powder, Raman spectroscopy confirmed the presence of the Ta_6Br_{12} cluster core in the film (Fig. S3 in the ESI†).

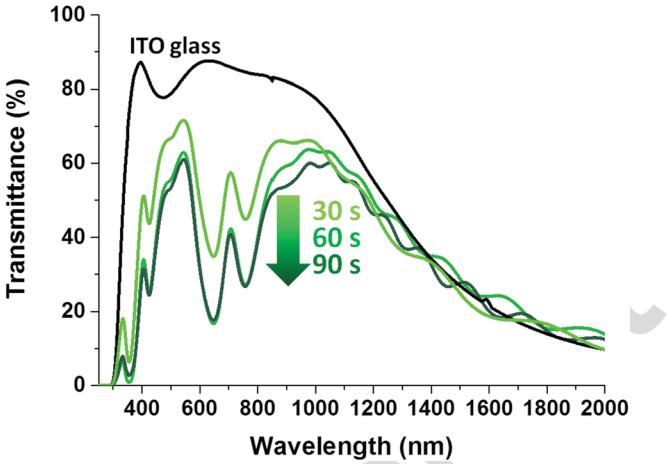

Fig. 6 UV-vis-NIR transmission spectra of the ITO substrate and the green-Ta_6@PVP@ITO films on 1 × 2.5 cm substrates obtained at 30 V and 30 s, 60 s and 90 s.

Thus, the optical properties of these green-Ta_6@PVP@ITO films were determined to be better than those obtained without PVP. Indeed, their transmittance of around 500 nm is greater than that of the green-Ta_6@ITO films. The two absorption peaks in the red region of around 650 and 750 nm characteristic of the green $[Ta_6Br^i_{12}]^{2+}$ species are stronger. This translates into few scattering phenomena and a strong coloration of the green-Ta_6@PVP@ITO films. The results for T_{vis}, T_{sol}, and T_{vis}/T_{sol} and the color coordinates (x, y, and z) of the green-Ta_6@PVP@ITO films are reported in Table 1 and Fig. 4 and were compared to the previous ones (the UV-vis-NIR spectra and the FOM values for the green-Ta_6@PVP@ITO films after several weeks of exposure in air are reported in Fig. S4 and Table S4 in the ESI†). The green-Ta_6@PVP@ITO film clearly has a high impact in terms of T_{sol} with a small increase in the ratio of T_{vis}/T_{sol}. Thus, the incorporation of PVP into the green-Ta_6@ITO film is clearly beneficial for the optical properties with a T_{vis}/T_{sol} ratio equal to 1.25. The deposition process was also performed on a 4 × 5 cm ITO glass substrate and the film showed a high transparency, which indicates the possible scalability of the EPD process (Fig. S7, ESI†).

D Conclusions

In summary, we fabricated the first transparent films based on the Ta_6 metal clusters for UV and NIR blocking static applications by a low-cost EPD solution process. The EPD process allowed the fabrication of micron-thick films in a very short time (less than 1 min) with a high thickness control. Transparent and homogeneous red-brown TBH films were easily obtained in acetone due to the simple stabilization of the red-brown $[Ta_6Br^i_{12}]^{3+/4+}$ cluster species, and thus the realization of homogeneous transparent green films required specific conditions. It was performed by the addition of a small amount of water leading to the stabilization of the green $[Ta_6Br^i_{12}]^{2+}$ species. However, it appears necessary to have high control over the water concentration. Indeed, it drastically impacts the growth of the Ta_6-based particles,

Revised manuscript

and thus the film morphology limits their transparency. However, we succeeded in overcoming this water effect by the addition of a small amount of PVP as a binder leading to a much better thin film deposition. Finally, the resulting green-Ta_6@PVP@ITO film combined the IR reflecting properties of ITO and the UV-NIR absorption properties of the clusters. This study demonstrated that metal atom clusters are new promising UV-NIR blocking pigments which allow (i) the production of highly transparent ITO glass with a deep emerald-green colour with a few microns thick coating, and (ii) increased filtering of the most energetic UV-NIR radiation.

Conflicts of interest

There are no conflicts to declare.

Acknowledgements

This study was carried out as part of the France–Japan International Collaboration Framework (UMI 3629-LINK Center). The authors wish to thank the people involved in LINK and related activities, particularly David Lechevalier and Dr Mari Kono of Saint-Gobain KK (Tokyo, Japan). The study was financially supported by Saint-Gobain (France), CNRS, Université de Rennes 1, and NIMS through the Laboratory for Innovative Key Materials and Structures (LINK UMI 3629). Raman investigations were performed using the facilities available on the "Spectroscopie et Imagerie Raman" (SIR) Platform from UMS 2001 CNRS-Université Rennes 1. The authors are very grateful to Bertrand Lefeuvre from ISCR UMR 6226 CNRS-Université Rennes 1 and Alain Moréac from IPR UMR 6252 CNRS-Université Rennes 1.

Notes and references

1 N. S. Lewis and D. G. Nocera, *Proc. Natl. Acad. Sci. U. S. A.*, 2006, **103**, 15729; International Energy Agency, World Enery Outlook, 2016.

2 C. G. Granqvist, *Thin Solid Films*, 2014, **564**, 1; E. Lichtfouse, *Sustainable Agriculture Reviews*, Springer, 2015; F. Pacheco-Torgal, J. Labrincha, L. Cabeza and C. G. Granqvist, *Eco-efficient Materials for Mitigating Building Cooling Needs: Design, Properties and Applications*, Woodhead Publishing, 2015; R. W. Johns, H. A. Bechtel, E. L. Runnerstrom, A. Agrawal, S. D. Lounis and D. J. Milliron, *Nat. Commun.*, 2016, **7**, 11583.

3 Y. Cao, J.-H. Dou, N.-J. Zhao, S. Zhang, Y.-Q. Zheng, J.-P. Zhang, J.-Y. Wang, J. Pei and Y. Wang, *Chem. Mater.*, 2017, **29**(2), 718.

4 A. Llordes, G. Garcia, J. Gazquez and D. J. Milliron, *Nature*, 2013, **500**, 323; I. Trenque, S. Mornet, E. Duguet, J. Majimel, A. Brûll, K. Teinz, E. Kemnitz and M. Gaudon, *Opt. Mater.*, 2013, **35**, 661; S. Y. Li, G. A. Niklasson and C. G. Granqvist, *J. Appl. Phys.*, 2014, **115**, 053513; T. E. Williams, C. M. Chang, E. L. Rosen, G. Garcia, E. L. Runnerstrom, B. L. Williams, B. Koo, R. Buonsanti, D. J. Milliron and B. A. Helms, *J. Mater. Chem. C*, 2014, **2**, 3328; A. Llordés, Y. Wang, A. Fernandez-Martinez, P. Xiao, T. Lee, A. Poulain, O. Zandi, C. A. Saez Cabezas, G. Henkelman and D. J. Milliron, *Nat. Mater.*, 2016, **15**, 1267.

5 G. B. Smith, C. A. Deller, P. D. Swift, A. Gentle, P. D. Garrett and W. K. Fisher, *J. Nanopart. Res.*, 2002, **4**, 157; S. Schelm, G. B. Smith, P. D. Garrett and W. K. Fisher, *J. Appl. Phys.*, 2005, **97**, 124314; N. L. Stokes, J. A. Edgar, A. M. McDonagh and M. B. Cortie, *J. Nanopart. Res.*, 2010, **12**, 2821; M. Carboni, M. Carravetta, X. L. Zhang and E. Stulz, *J. Mater. Chem. C*, 2016, **4**, 1584.

6 A. Renaud, M. Wilmet, T. G. Truong, M. Seze, P. Lemoine, N. Dumait, W. Chen, N. Saito, T. Ohsawa, T. Uchikoshi, N. Ohashi, S. Cordier and F. Grasset, *J. Mater. Chem. C*, 2017, **5**, 8160.

7 M. Holgado, F. García-Santamaría, A. Blanco, M. Ibisate, A. Cintas, H. Míguez, C. J. Serna, C. Molpeceres, J. Requena, A. Mifsud, F. Meseguer and C. López, *Langmuir*, 1999, **15**, 4701; G. Anné, K. Vanmeensel, J. Vleugels and O. Van der Biest, *Colloids Surf., A*, 2004, **245**, 35; S. Dor, S. Rühle, A. Ofir, M. Adler, L. Grinis and A. Zaban, *Colloids Surf., A*, 2009, **342**, 70; D. Hanaor, M. Michelazzi, P. Veronesi, C. Leonelli, M. Romagnoli and C. Sorrell, *J. Eur. Ceram. Soc.*, 2011, **31**, 1041; R. Kawakami, T. Yuasa, K. Ito, Y. Sato, Y. Mori, M. Adachi and S. Yoshikado, *J. Aust. Ceram. Soc.*, 2012, **48**, 236; L. A. Ma and T. L. Guo, *Ceram. Int.*, 2013, **39**, 6923; Y. Huang, D. K. Sarkar and X.-G. Chen, *Appl. Surf. Sci.*, 2015, **327**, 327.

8 B. Gao, G. Z. Yue, Q. Qiu, Y. Cheng, H. Shimoda, L. Fleming and O. Zhou, *Adv. Mater.*, 2001, **13**, 1770; A. R. Boccaccini, J. Cho, J. A. Roether, B. J. C. Thomas, E. J. Minay and M. S. P. Shaffer, *Carbon*, 2006, **44**, 3149; J. Cho, K. Konopka, K. Rozniatowski, E. García-Lecina, M. S. P. Shaffer and A. R. Boccaccini, *Carbon*, 2009, **47**, 58; Z.-S. Wu, S. Pei, W. Ren, D. Tang, L. Gao, B. Liu, F. Li, C. Liu and H.-M. Cheng, *Adv. Mater.*, 2009, **21**, 1756.

9 H. Zhu, H. Liu, I. Zhitomirsky and S. Zhu, *Mater. Lett.*, 2015, **142**, 19; I. Hod, W. Bury, D. M. Karlin, P. Deria, C. W. Kung, M. J. Katz, M. So, B. Klahr, D. Jin, Y. W. Chung, T. W. Odom, O. K. Farha and J. T. Hupp, *Adv. Mater.*, 2014, **26**, 6295; C. Streich, S. Koenen, M. Lelle, K. Peneva and S. Barcikowski, *Appl. Surf. Sci.*, 2015, **348**, 92.

10 J. Liu, Z. Wu, T. Li, D. Zhou, K. Zhang, Y. Sheng, J. Cui, H. Zhang and B. Yang, *Nanoscale*, 2016, **8**, 395.

11 Y. Sakka and T. Uchikoshi, *KONA Powder Part. J.*, 2010, **28**, 74; J. Fabian, *Dyes Pigm.*, 2010, **84**, 36.

12 M. B. Robin and N. A. Kuebler, *Inorg. Chem.*, 1965, **4**, 978; R. B. Burbank, *Inorg. Chem.*, 1966, **5**, 1491; B. G. Hughes, J. L. Meyer, P. B. Fleming and R. E. Mc Carley, *Inorg. Chem.*, 1970, **9**(6), 1343.

13 R. W. Murray, *Chem. Rev.*, 2008, **108**, 2705.

14 H. X. Xu and K. S. Suslick, *Adv. Mater.*, 2010, **22**, 3209; H.-T. Sun and Y. Sakka, *Sci. Technol. Adv. Mater.*, 2014, **15**, 014205; K. Costuas, A. Garreau, A. Bulou, B. Fontaine, J. Cuny, R. Gautier, M. Mortier, Y. Molard, J.-L. Duvail, E. Faulques and S. Cordier, *Phys. Chem. Chem. Phys.*, 2015, **17**, 28574; B. Dierre, K. Costuas, N. Dumait, S. Paofai, M. Amela-Cortes, Y. Molard, F. Grasset, Y. Cho, K. Takahashi, N. Ohashi,

Revised manuscript

T. Uchikoshi and S. Cordier, *Sci. Technol. Adv. Mater.*, 2017, **18**(1), 458.

15 M. Turner, V. B. Golovko, O. P. Vaughan, P. Abdulkin, A. Berenguer-Murcia, M. S. Tikhov, B. F. Johnson and R. M. Lambert, *Nature*, 2008, **454**, 981.

16 T. Aubert, F. Cabello Hurtado, M. A. Esnault, C. Neaime, D. Lebret-Chauvel, S. Jeanne, P. Pellen, C. Roiland, L. Le Polles, N. Saito, K. Kimoto, H. Haneda, N. Ohashi, F. Grasset and S. Cordier, *J. Phys. Chem. C*, 2013, **117**, 20154; K. Kirakci, V. Šícha, J. Holub, P. Kubàt and K. Lang, *Inorg. Chem.*, 2014, **53**, 13012; K. Kirakci, P. Kubàt, K. Fejfarovà, J. Martinčík, M. Nikl and K. Lang, *Inorg. Chem.*, 2016, **55**, 803; C. Neaime, M. Amela-Cortes, F. Grasset, Y. Molard, S. Cordier, B. Dierre, M. Mortier, T. Takei, K. Takahashi, H. Haneda, M. Verelst and S. Lechevallier, *Phys. Chem. Chem. Phys.*, 2016, **18**, 30166.

17 P. S. Kuttipillai, Y. Zhao, C. J. Traverse, R. J. Staples, B. G. Levine and R. R. Lunt, *Adv. Mater.*, 2016, **28**, 320; S. Cordier, F. Grasset, Y. Molard, M. Amela-Cortes, R. Boukherroub, S. Ravaine, M. Mortier, N. Ohashi, N. Saito and H. Haneda, *J. Inorg. Organomet. Polym.*, 2015, **25**, 189; T. G. Troung, B. Dierre, F. Grasset, N. Saito, N. Saito, T. K. N. Nguyen, K. Takahashi, T. Uchikoshi, M. Amela-Cortes, Y. Molard, S. Cordier and N. Ohashi, *Sci. Technol. Adv. Mater.*, 2016, **17**(1), 443.

18 A. Barras, S. Cordier and R. Boukherroub, *Appl. Catal., B*, 2012, **123**, 1; A. Barras, M. R. Das, R. R. Devarapalli, M. V. Shelke, S. Cordier, S. Szunerits and R. Boukherroub, *Appl. Catal., B*, 2013, **130**, 270.

19 A. Renaud, F. Grasset, B. Dierre, T. Uchikoshi, N. Ohashi, T. Takei, A. Planchat, L. Cario, S. Jobic, F. Odobel and S. Cordier, *ChemistrySelect*, 2016, **1**, 2284.

20 S. Nagashima, S. Kamiguchi and T. Chihara, *Metals*, 2014, **4**, 235.

21 D. Bauer and H.-G. von Schnering, *Z. Anorg. Allg. Chem.*, 1968, **361**, 259; S. Cordier, C. Perrin and M. Sergent, *Z. Anorg. Allg. Chem.*, 1993, **619**, 621; S. Cordier, C. Loisel, C. Perrin and M. Sergent, *J. Solid State Chem.*, 1999, **147**, 350; S. Kamiguchi, T. Mori, M. Watanabe, A. Suzuki, M. Kodomari, M. Nomurac, Y. Iwasawa and T. Chihara, *J. Mol. Catal. A: Chem.*, 2006, **253**, 176; M. N. Sokolov, P. A. Abramov, M. A. Mikhailov, E. V. Peresypkina, A. V. Virovets and V. P. Fedin, *Z. Anorg. Allg. Chem.*, 2010, **636**, 1543; J. König, I. Dartsch, A. Topp, E. Guillamón, R. Llusar and M. Köckerling, *Z. Anorg. Allg. Chem.*, 2016, **642**(7), 572.

22 W. H. Chapin, *J. Am. Chem. Soc.*, 1910, **32**, 323.

23 J. Löwe, D. Stock, B. Jap, P. Zwickl, W. Baumeister and R. Huber, *Science*, 1995, **268**, 533; P. Cramer, D. A. Bushnell, J. Fu, A. L. Gnatt, B. Maier-Davis, N. E. Thompson, R. R. Burgess, A. M. Edwards, P. R. David and R. D. Kornberg, *Science*, 2000, **288**, 640; K. N. Ferreira, T. M. Iverson, K. Maghlaoui, J. Barber and S. Iwata, *Science*, 2004, **303**, 1831.

24 B. F. Mullan, M. T. Madsen, L. Messerle, V. Kolesnichenko and J. Kruger, *Acad. Radiol.*, 2000, **7**, 254.

25 P. C. Chabrié, *Compt. Rend.*, 1907, **144**, 804.

26 R. E. McCarley, B. G. Hughes, F. A. Cotton and R. Zimmerman, *Inorg. Chem.*, 1965, **4**, 1491.

27 J. H. Espenson and R. E. McCarley, *J. Am. Chem. Soc.*, 1966, **88**, 1063.

28 B. Spreckelmeyer and H. Schäfer, *J. Less-Common Met.*, 1967, **13**, 127.

29 K. Ariga, Y. Yamauchi, G. Rydzek, Q. Ji, Y. Yonamine, K. C.-W. Wu and J. P. Hill, *Chem. Lett.*, 2014, **43**, 36; K. Ariga, A. Vinu, Y. Yamauchi, Q. Ji and J. P. Hill, *Bull. Chem. Soc. Jpn.*, 2012, **85**, 1.

30 F. W. Koknat, J. A. Parsons and A. Vongvusharintra, *Inorg. Chem.*, 1974, **13**, 1699; D. N. T. Hay and L. Messerle, *J. Struct. Biol.*, 2002, **139**, 147; M. N. Sokolov, P. A. Abramov, M. A. Mikhailov, E. V. Peresypkina, A. V. Virovets and V. P. Fedin, *Z. Anorg. Allg. Chem.*, 2010, **636**, 1543.

31 N. E. Cooke, T. Kuwana and J. H. Espenson, *Inorg. Chem.*, 1971, **10**, 1081.

32 R. Eisenbraun and H. Schäfer, *Z. Anorg. Allg. Chem.*, 1985, **530**, 222.

33 H. S. Harned, *J. Am. Chem. Soc.*, 1913, **35**, 1078.

34 T. K. N. Nguyen, F. Grasset, B. Dierre, C. Matsunaga, S. Cordier, P. Lemoine, N. Ohashi and T. Uchikoshi, *ECS J. Solid State Sci. Technol.*, 2016, **5**, R178.

35 W. D. Ristenpart, I. A. Aksay and D. A. Saville, *Phys. Rev. E: Stat., Nonlinear, Soft Matter Phys.*, 2004, **69**, 021405.

36 V. R. Estrelolopis, Z. R. Ulberg and S. A. Koniashvili, *Colloid J. USSR*, 1982, **44**, 74.

37 K. M. Koczkur, S. Mourdikoudis, L. Polavarapu and S. E. Skrabalak, *Dalton Trans.*, 2015, **44**, 17883; Y. Xiong, H. Cai, B. J. Wiley, J. Wang, M. J. Kim and Y. Xia, *J. Am. Chem. Soc.*, 2007, **129**, 3665; T. Aubert, N. Nerambourg, N. Saito, H. Haneda, N. Ohashi, M. Mortier, S. Cordier and F. Grasset, *Part. Part. Syst. Charact.*, 2013, **30**, 90; M. Sivakumar, S. Kanagesan, V. Umapathy, R. S. Babu and S. Nithiyanantham, *J. Supercond. Novel Magn.*, 2013, **26**, 725.

Revised manuscript